High-resolution electron-momentum spectroscopy of the valence orbitals of the benzene molecule

Yanru Huang,* Guojun Cai, and Jing Yu
College of Science, Liaoning Shihua University, Fushun 113001, China

(Received 8 August 2018; published 17 October 2018)

The binding-energy spectrum and electron-momentum spectra of valence orbitals of benzene were measured via a high-resolution electron-momentum spectrometer at incident energies of 600 and 1200 eV plus the binding energy. The experimental momentum profiles were compared with the results from a plane-wave impulse approximation (PWIA) calculation using Dyson orbitals obtained from symmetry-adapted-cluster configuration-interaction calculations. For the $1e_{1g}$, $3e_{2g}$, $3e_{1u}$, and $2b_{1u}$ orbitals, the discrepancy between the experimental distributions and the PWIA calculations was tentatively assigned to the distorted wave effects. The current high-resolution electron-momentum spectroscopy results provide the experimental benchmark for rigorous distorted-wave calculations about benzene in the future.

DOI: 10.1103/PhysRevA.98.042705

I. INTRODUCTION

Electron-momentum spectroscopy (EMS) is based on kinematically complete $(e, 2e)$ electron impact ionization [1]. A bound electron of the target atom or molecule is knocked out by the incident electron, and the incident electron itself is scattered off. EMS is a powerful tool for studying the electronic structures of atoms, molecules, and solids [1–9], and for investigating electron collision dynamics [10–16]. Within the plane-wave impulse approximation (PWIA) [1,17], the measured $(e, 2e)$ cross section is directly proportional to the modular squaring of the momentum-space wave function of the ionized electron and does not depend on the incident-electron impact energy [1]. Many experimental and theoretical works on atoms and small molecules have shown that the PWIA is usually valid for impact energies in the keV range [10,11]. However, it was recently found that the PWIA is not valid for several molecular orbitals with a high symmetry, such as the $^2\Pi_g$ orbital of oxygen molecule O_2 [17], the $1E_g$ orbital of ethane C_2H_6 [18], the $1b_{3g}$ orbital of ethylene C_2H_4 [19], and all valence orbitals of sulfur hexafluoride SF_6 [20]. In these valence orbital momentum profiles, the PWIA calculation underestimated the $(e, 2e)$ ionization intensities in the low-momentum region and cannot explain the observed impact-energy-dependent effects. It is an interesting question whether there is a similar effect for the high-symmetric benzene molecule C_6H_6.

Benzene C_6H_6 is a fundamental aromatic molecule with a D_{6h} symmetry. Its electronic structures have been extensively studied via photoelectron spectroscopy with He I [21–23] and He II radiation [24,25], as well as x ray [26]. The measured spectra have been interpreted and assigned by several theoretical calculations [27–29]. In 1981, Fuss *et al.* first measured the $(e, 2e)$ ionization spectrum of benzene at an impact electron of 1200 eV [30]. Later, Samardzic *et al.* reported its complete valence orbital momentum distributions in 1993 [31]. However, the low statistical accuracy and the relative low-energy resolution (full width at half maximum of 1.7 eV) of these measurements prevented them from observing the distorted wave effects. Here, we report a high- resolution electron-momentum spectroscopy study for molecular benzene.

The experiment was conducted on the high-resolution electron-momentum spectrometer ($\Delta\theta = \pm 0.53^\circ$, $\Delta\phi = \pm 0.84^\circ$, $\Delta E = 0.68$ eV) at Tsinghua University [32–35]. In order to examine the validity of the PWIA and the influence of the distorted-wave effects, the momentum distributions of valence orbitals of benzene were measured at impact energies of 600 and 1200 eV plus the binding energy. The high-level symmetry-adapted-cluster configuration-interaction (SAC-CI) method [36,37] and the density functional theory (DFT) method with the hybrid Becke three-parameter Lee-Yang-Parr (B3LYP) functional [38,39] were employed to interpret the binding-energy spectra and the electron-momentum distributions.

II. EXPERIMENTAL AND THEORETICAL METHODS

The third generation EMS spectrometer at Tsinghua University features high coincidental count rate and high-energy resolution. The details of the spectrometer have been reported in previous works [32–35]. Briefly, the spectrometer takes symmetric noncoplanar geometry; i.e., the two outgoing electrons have almost equal energies and equal polar angles ($\theta_1 = \theta_2 = 45^\circ$) with respect to the direction of the incident electron beam. An electron gun equipped with an oxide cathode can provide a collimated electron beam with a lower-energy spread and a lower divergence angle than the generic filament cathode. A molybdenum aperture was introduced to constrain the electron beam to 0.3-mm diameter. With the calibration measurements for the Ar $3p$ orbital, the present energy resolution was measured as 0.68 eV at the impact energy of 1200 eV (see Fig. 6 in Ref. [34] for details). The azimuthal angle resolution $\Delta\phi$ is $\pm 0.84^\circ$, and the acceptance of the polar angle $\Delta\theta$ is $\pm 0.53^\circ$. A double-toroidal energy analyzer equipped with two-dimensional position sensitive

*huangganen12@sina.cn

detectors greatly enhances the sensitivity of the spectrometer. A commercial C_6H_6 sample with a claimed purity of 99.8% was directly used without further purification. The absorbed gas was removed through three recycles of freezing-pump–thaw process. The needle valve, which is used to control the flow rate of benzene from the reservoir to the $(e,\ 2e)$ interaction region, was heated to ∼60 °C in order to prevent the fluctuation of the flow rate due to the possible condensation of benzene.

The initial momentum (p) of the knocked-out electron can be monitored by scanning the azimuthal angle (ϕ) under which the electrons are selected, according to basic conservation laws on energies and momenta [1]:

$$p = \left[(p_0 - 2p_1\cos\theta)^2 + 4p_1^2\sin^2\theta\sin^2\frac{\phi}{2}\right]^{1/2} \quad (1)$$

where p_0 and p_1 are the momenta of the incident and outgoing electrons, respectively.

Under the assumptions of the Born, binary encounter, and plane-wave impulse approximations, the differential cross section for randomly oriented gas-phase target atoms or molecules is [1]

$$\sigma_{\mathrm{EMS}} \propto S_i^f \int d\Omega \left|\left\langle e^{-ipr}\Psi_f^{N-1} \mid \Psi_i^N\right\rangle\right|^2 \quad (2)$$

where S_i^f represents the spectroscopic factor, e^{-ipr} stands for the plane wave, and Ψ_i^N and Ψ_f^{N-1} are the wave functions of the ground state and the ionized state of the molecule, respectively. $\langle\Psi_f^{N-1} \mid \Psi_i^N\rangle$ is also named the Dyson orbital. N is the total electron number. $\int d\Omega$ represents the spherical average over the random orientation of molecules. In the present paper, the SAC-CI method [36,37] was employed to calculate the Dyson orbital [40–42], which was performed with the GAUSSIAN 03 program [43]. Fourier transformations and the spherical average of momentum distributions for each Dyson orbital were calculated with a home-compiled NEMS program [44]. With the target Kohn-Sham approximation (TKSA) [11,12,45], the above equation can be simplified as [1]

$$\sigma \propto \int d\Omega \left|\psi_j^{\mathrm{KS}}(p)\right|^2 \quad (3)$$

where $\psi_j^{\mathrm{KS}}(p)$ is the momentum space Kohn-Sham orbital for the jth electron.

III. RESULTS AND DISCUSSIONS

The benzene molecule contains 42 electrons. At the B3LYP/aug-cc-pVTZ level, the electronic configuration of its ground state is

$$\underbrace{(2a_{1g})^2(2e_{1u})^4(2e_{2g})^4}_{\text{Inner-valence}}\underbrace{(3a_{1g})^2(2b_{1u})^2(1b_{2u})^2(3e_{1u})^4(1a_{2u})^2(3e_{2g})^4(1e_{1g})^4}_{\text{Outer-valence}}.$$

Figure 1 shows the molecular orbitals for benzene. It can be seen that except for the $3a_{1g}$ and $2a_{1g}$ orbitals all other orbitals have antisymmetry. The antisymmetric orbital has zero intensity at the momentum origin ($p = 0$ a.u.) in the momentum space. The previous studies showed that the distorted wave effect is usually more notable for an antisymmetric orbital [17–20,46,47]. The experimental momentum distributions have higher intensity at the low-momentum region than the PWIA calculations. This increased low-momentum intensity is usually labeled as the "turn-up" effect in EMS [47]. The degree of the turn-up depends on the impact energy.

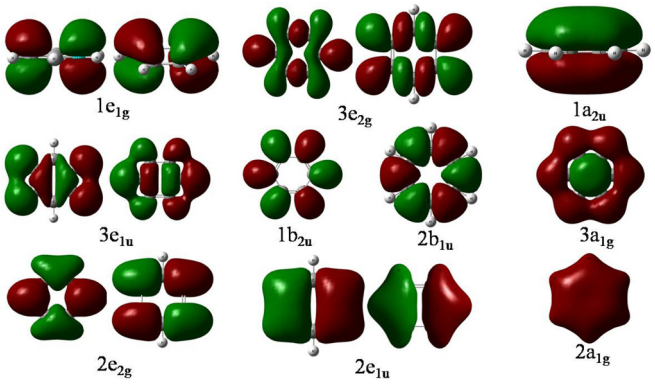

FIG. 1. The valence molecular orbitals of benzene.

Figure 2 presents the measured binding-energy spectra of benzene in comparison with the simulation using the SAC-CI method. The experimental energy spectrum was obtained by summing over all the azimuthal angles ϕ. To extract the momentum distribution for each orbital, the binding-energy spectra at different azimuthal angles ϕ were fitted using Gaussian functions. The peak centers were determined through high-resolution PES, and the widths were determined by combining the experimental energy resolution and the vibrational broadening in PES. The experimental ionization energies and the calculated values (the ionization energies and pole strengths) are compared in detail in Table I. In general, except for orbital $1e_{1g}$, the SAC-CI calculation is in good agreement with the experimental binding-energy spectrum.

The first well-isolated peak at 9.4 eV is the ionization from the $1e_{1g}$ orbital. The SAC-CI calculation predicted it to be 8.62 eV, which is a significant underestimation. Such rather severe discrepancies between the experimentally apparent and the vertical transition energies may be attributable to strong vibronic coupling interactions, which can lead to a collapse of the Born-Oppenheimer approximation. Reference [23] shows that the $1e_{1g}$ (π_1^{-1}) state photoelectron band is dominated by the intense, asymmetric, and sharp 0-0 main peak at 9.2431 eV followed by a number of weak vibrational structures, which is in accordance with the above explanation. Peaks 2 and 3 in the $(e,\ 2e)$ binding-energy spectrum are associated ionizations from the $3e_{2g}$ and $1a_{2u}$ molecular orbitals, respectively. The next noticeable feature is a composite spectral band extending

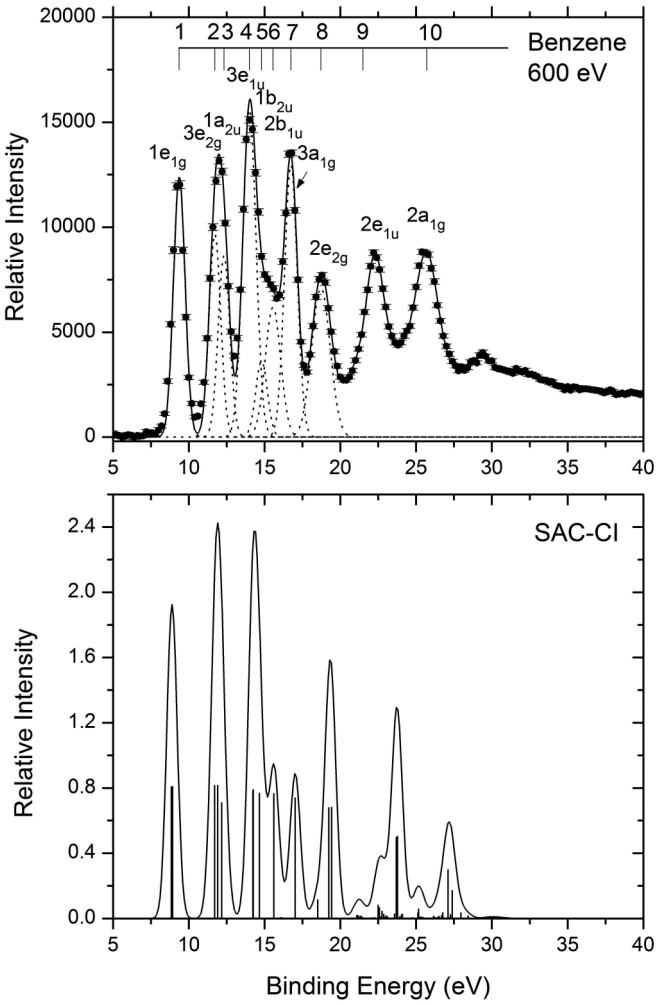

FIG. 2. Experimental binding-energy spectra summed over all ϕ angles at the impact energy of 600 eV plus binding energies (top). The ionization spectrum was simulated using the SAC-CI general-R method with the aug-cc-pVTZ basis set (bottom). The heights of the sticks under the curve represent the spectroscopic factors.

TABLE I. Benzene ionization potentials (eV) and spectroscopic factors (in parentheses). Only states having pole strengths $\geqslant$0.05 are included.

State	PES[a]	EMS[b]	EMS[c]	GF[b]	ADC(3)[b]	SAC-CI[c]
$1e_{1g}$	9.44	9.3	9.4	9.1	9.05(0.88)	8.62(0.84)
$3e_{2g}$	11.62	11.6	11.7	11.95	12.07(0.90)	11.80 (0.87)
$1a_{2u}$	12.39	12.4	12.4	12.26	12.26(0.75)	12.22 (0.71)
					16.78(0.16)	S 17.20 (0.20)
$3e_{1u}$	13.93	14.0	14.1	14.46	14.35(0.87)	14.17 (0.83)
$1b_{2u}$	14.81	15.1	14.8	14.83	14.95(0.87)	14.68 (0.81)
$2b_{1u}$	15.43	15.1	15.6	15.75	15.66(0.84)	15.61 (0.80)
$3a_{1g}$	16.84	16.9	16.9	17.15	17.27(0.79)	17.04 (0.76)
					21.87(0.05)	21.85(0.05)
$2e_{2g}$	19.12	19.2	19.0	19.6	19.03(0.09)	19.33(0.08)
					19.12(0.13)	19.52(0.55)
					19.53(0.36)	19.88(0.22)
					20.00(0.09)	21.58(0.06)
					21.30(0.08)	21.69(0.28)
					23.23(0.15)	21.88(0.07)
$2e_{1u}$	22.6	22.6	22.6	24.6	23.39(0.38)	23.35(0.08)
					23.68(0.07)	23.68(0.39)
					23.93(0.20)	23.76(0.25)
$2a_{1g}$	25.9	25.9	26.0	28.7	26.44(0.13)	
					26.86(0.21)	
					27.09(0.07)	27.10(0.08)
					27.42(0.07)	27.23(0.06)
					29.16(0.05)	

[a]See Ref. [23].
[b]See Ref. [31].
[c]The present paper.

from 14.0 to 17.0 eV, exhibiting four peaks at 14.1, 14.8, 15.6, and 16.9 eV. Peaks 4, 5, and 6 essentially correspond to a one-electron ionization line originating from the $3e_{1u}$, $1b_{2u}$, and $2b_{1u}$ orbitals, respectively. The $3a_{1g}$ orbital at 16.9 eV corresponds to a single ionization peak and defines the border of the outer-valence region of the $(e,\ 2e)$ binding-energy spectrum of benzene. In addition, the present SAC-CI calculation predicted a rather intense shake-up line S with a pole strength of 0.20, at the binding energy of 17.20 eV, which corresponds to the ${1e_{1g}}^{-2}{1e_{2u}}^{+1}$ transition in the π-band system.

In the inner-valence region (19.0–40.0 eV), the energy spectrum is composed of three main peaks—$3a_{1g}$, $2e_{2g}$, and $2e_{1u}$ orbitals and the complicated satellite lines. According to the calculated SAC-CI results, peak 10 at 26.0 eV can be ascribed to a set of congested shake-up lines produced by orbitals $2e_{1u}$ and $2a_{1g}$. The vertical double-ionization energy threshold of benzene is located at -29.5 eV. Therefore, all computed shake-up states at binding energies above this threshold are subject to decay via the spontaneous emission of a second electron and should be regarded as resonances in a continuum of shake-off states, corresponding to a very long shake-off tail.

Since the experimental intensity is on a relative scale, a normalization procedure is needed. A global normalization factor was determined by fitting the summed experimental distributions of peaks 1–7 to the corresponding PWIA distributions. Then, this factor is used for normalization of each outer valence orbital. Figure 3 shows the experimental momentum distributions of the highest occupied molecular orbital $1e_{1g}$ in comparison with the DFT and SAC-CI calculations. The momentum profile for orbital $1e_{1g}$ of benzene exhibits a p-type symmetry, with the minimum in the electron density at $p = 0$ and the maximum located around $p = 0.75$ a.u. It can be seen that although all of the theoretical profiles correctly predict the general shape of the experimental profile a significant discrepancy was observed. The theoretical calculations fail to reproduce a significant turn-up of the $(e,\ 2e)$ ionization intensities at momenta below 0.5 a.u. Furthermore, the experimental momentum distribution in the low momentum region at 600 eV shows an unremarkable difference from that of 1200 eV. Because $1e_{1g}$ of the benzene ionization line is well isolated from the next cationic state $3e_{2g}$, it is unlikely that the discrepancies are due to the overlap from other states. The vibration and Jahn-Teller effects can partly explain the turn-up [3,41,48–56]. However, it cannot explain why the discrepancy depends on the impact energy. It is interesting to note that

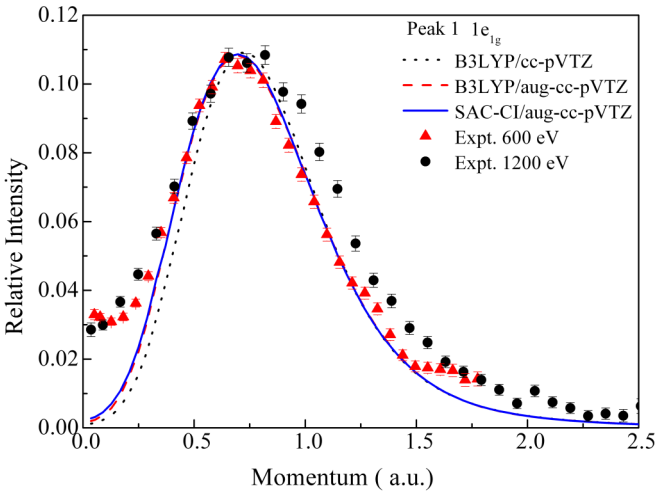

FIG. 3. Momentum distributions of peak 1.

the highest occupied molecular orbital is a classical d-like orbital. Therefore, it is reasonable to ascribe this turn-up to the distorted wave effects.

The experimental and theoretical EMS momentum distributions for peaks 2–7 are shown in Fig. 4. The three theoretical momentum profiles in Fig. 4(a) indicate that the $3e_{2g}$ orbital of benzene has a double-hump momentum distribution, which corresponds to the three nodal surfaces across the ring backbone of benzene. It can be seen that the calculated results only correctly predict the position of the first hump, but significantly underestimate the experimental intensities in the low momentum region ($p < 1.0$ a.u.). In the previous EMS investigation [31], Samardzic *et al.* thought that the poor agreement between the orbital $3e_{2g}$ experimental and calculated momentum distribution is due to the limitations of their SCF wave-function and basis sets. However, there is no notable difference between the B3LYP/aug-cc-pVTZ and the high level SAC-CI calculations. And, the B3LYP calculation with a larger basis set aug-cc-pVTZ produces almost the same distribution with the smaller basis set cc-pVTZ. Therefore, the discrepancy is unlikely due to the limitations of the wave function. In Fig. 4(b), there is also a notable discrepancy between theoretical predictions and experimental results for the orbital $1a_{2u}$. Since peak 2 overlaps peak 3, the deconvolution procedure may not separate their intensity cleanly. Therefore, the theoretical momentum distributions for the sum of $3e_{2g}$ and $1a_{2u}$ orbitals are compared with EMS measurements in Fig. 4(c). The agreement between theories and experiment improves, but the discrepancy in the low momentum region ($p < 0.3$ a.u.) still exists.

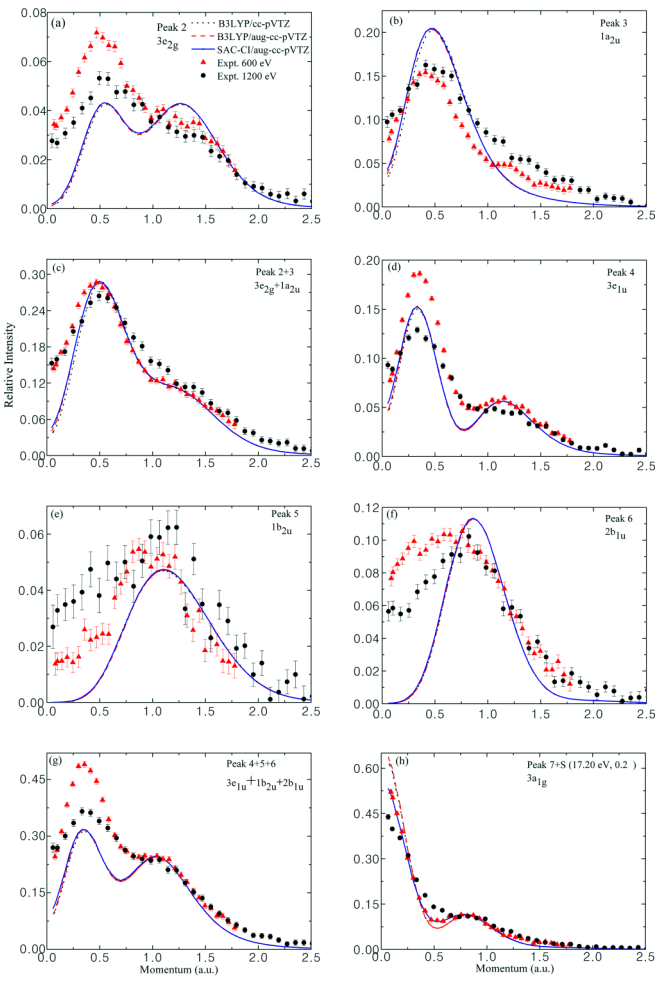

FIG. 4. Momentum distributions of peaks 2–7.

The momentum distribution of the orbital $3e_{1u}$ orbital in Fig. 4(d) exhibits two inequivalent humps. The theoretical calculations can roughly reproduce the overall profile of experimental distributions. However, the PWIA predictions significantly deviate from the experimental results at low momentum. The normalized experimental intensity for $p <$ 0.7 a.u. depends on the impact energy of electrons. The experimental intensity at the impact energy 600 eV is higher than the predictions, and becomes lower at 1200 eV. In the case of peaks 4–6 (binding-energy range of 14.1–15.6 eV), the energy separation between orbitals is quite small. The interference from the neighboring peaks cannot be excluded cleanly. For this reason, a sum of fitted peaks 4–6 has been considered and is compared in Fig. 4(g) with theoretical profiles for the sum of molecular orbitals. It can be seen that the discrepancy is still there. The experimental intensities are higher than the theoretical calculations in the low momentum region ($p < 0.5$ a.u.). The turn-up becomes lower as the impact energy increases from 600 to 1200 eV, which is consistent with the distortion effects. The distorted wave calculation for molecule C_6H_6 at high impact energy (~ 1 keV) is still a challenge due to the multicenter density distribution. A recent multicenter distorted-wave (MCDW) method [57–59] developed for high impact energies is expected to become a suitable model for EMS for investigating the distorted-wave effect in the future. In the PWIA calculation, the distortion interactions for all continuum electron wave functions are neglected. Within the MCDW method, the fast incoming and outgoing electrons are described by the plane waves, while the slow ejected electron is described by the multicenter distorted wave, which is solved from the anisotropic multicenter potential between the ejected electron and the ionic molecule. The MCDW method is universal and inexpensive for electron-impact single ionization of a molecular system in the coplanar-asymmetric kinematics.

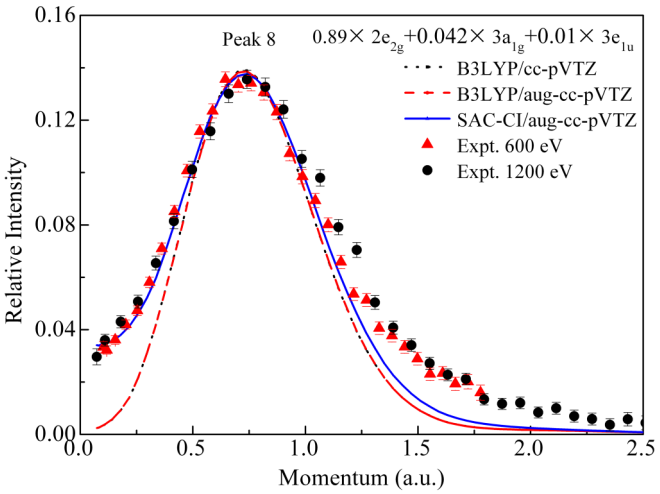

FIG. 5. Momentum distributions of peak 8.

According to the SAC-CI calculation and high-resolution PES, peak 7 at 16.9 eV includes one-electron contributions from the outer valence orbital $3a_{1g}$ and the $\pi^{-2}\pi*^{+1}$ satellite line S (17.20 eV, pole strength equals 0.20) of the $1a_{2u}$ orbital. As shown in Fig. 4(h), the theoretical predictions can describe the experimental momentum distributions.

Peaks 8–10 are related to the inner valence orbitals $2e_{2g}$, $2e_{1u}$, and $2a_{1g}$ and their satellite lines. The congested satellite lines form a continuum background, which mixes with the main lines of $2e_{1u}$ and $2a_{1g}$. It is hard to obtain their experimental momentum distribution individually. Only the experimental momentum distribution for the first inner valence ionization channel at 19.2 eV, arising from ionization from orbital $2e_{2g}$, is analyzed in Fig. 5. According to the high level SAC-CI calculation and PES, the experimental momentum distributions of peak 8 are compared with the composed theoretical results $0.89 \times 2e_{2g} + 0.042 \times 3a_{1g} + 0.01 \times 3e_{1u}$. The calculations can reproduce well the experimental momentum distributions.

IV. CONCLUSIONS

EMS measurements of benzene over the whole valence region were performed using a high-resolution binary $(e, 2e)$ electron-momentum spectrometer ($\Delta E = 0.68$ eV, $\Delta\theta = \pm 0.53^\circ$, $\Delta\phi = \pm 0.84^\circ$) at electron impact energies of 600 and 1200 eV, respectively, and were analyzed with high level SAC-CI calculation. The theoretical calculations based on the SAC-CI/aug-cc-pVTZ with PWIA cannot reproduce well the experimental momentum distributions. The discrepancy depends on the impact energy of electrons, which is qualitatively consistent with the distorted wave effects.

ACKNOWLEDGMENTS

This work was supported by the Young Scientists Fund of the National Natural Science Foundation of China (Grants No. 11404154 and No. 11304136). The authors also acknowledge help from Prof. Ning at Tsinghua University.

[1] E. Weigold and I. E. McCarthy, *Electron Momentum Spectroscopy* (Kluwer, New York, 1999).
[2] J. S. Zhu, J. K. Deng, and C. G. Ning, Phys. Rev. A **85**, 052714 (2012).
[3] Y. R. Miao, J. M. Li, J. K. Deng, and C. G. Ning, J. Electron Spectrosc. Relat. Phenom. **193**, 1 (2014).
[4] E. L. Wang, X. Shan, Y. F. Shi, Y. G. Tang, and X. J. Chen, Rev. Sci. Instrum. **84**, 123110 (2013).
[5] J. K. Deng, and C. G. Ning, J. Electron Spectrosc. Relat. Phenom. **161**, 43 (2007).
[6] X. G. Ren, C. G. Ning, J. K. Deng, S. F. Zhang, and G. L. Su, Chem. Phys. Lett. **397**, 82 (2004).
[7] Z. Zhang, X. Shan, T. Wang, E. L. Wang, and X. J. Chen, Phys. Rev. Lett. **112**, 023204 (2014).
[8] Z. J. Li, X. J. Chen, X. Shan, T. Liu, and K. Z. Xu, J. Chem. Phys. **130**, 054302 (2009).
[9] C. G. Ning, Y. R. Huang, S. F. Zhang, J. K. Deng, K. Liu, Z. H. Luo, and F. Wang, J. Phys. Chem. A **112**, 11078 (2008).
[10] C. E. Brion, Int. J. Quantum Chem. **29**, 1397 (1986).
[11] I. E. McCarthy and E. Weigold, Rep. Prog. Phys. **54**, 789 (1991).
[12] M. A. Coplan, J. H. Moore, and J. P. Doering, Rev. Mod. Phys. **66**, 985 (1994).
[13] M. Takahashi, Bull. Chem. Soc. Jpn. **82**, 751 (2009).
[14] C. J. Colyer, M. A. Stevenson, O. Al-Hagan, D. H. Madison, C. G. Ning, and B. Lohmann, J. Phys. B **42**, 235207 (2009).
[15] K. L. Nixon, A. J. Murray, H. Chaluvadi, S. Amami, D. H. Madison, and C. G. Ning, J. Chem. Phys. **136**, 094302 (2012).
[16] H. Chaluvadi, C. G. Ning, and D. Madison, Phys. Rev. A **89**, 062712 (2014).
[17] C. G. Ning, X. G. Ren, J. K. Deng, G. L. Su, S. F. Zhang, and G. Q. Li, Phys. Rev. A **73**, 022704 (2006).
[18] X. G. Ren, C. G. Ning, J. K. Deng, S. F. Zhang, G. L. Su, Y. R. Huang, and G. Q. Li, J. Electron Spectrosc. Relat. Phenom. **151**, 92 (2006).
[19] X. G. Ren, C. G. Ning, J. K. Deng, S. F. Zhang, G. L. Su, F. Huang, and G. Q. Li, Phys. Rev. Lett. **94**, 163201 (2005).
[20] X. Wang, S. Xu, C. Ning, O. Al-Hagan, P. Hu, Y. Zhao, Z. Xu, J. Deng, E. Wang, X. Ren, A. Dorn, and D. Madison, Phys. Rev. A **97**, 062704 (2018).
[21] B. Jonsson and E. Lindholm, Ark. Fyr. **39**, 65 (1969).
[22] L. Asbrink, E. Lindholm, and O. Fdquis, Chem. Phys. Lett. **5**, 609 (1970).
[23] P. Baltzer, L. Karlsson, B. Wannberg, G. Ohrwall, D. M. P. Holland, M. A. MacDonald, M. A. Hayes, and W. von Niessen, Chem. Phys. **224**, 95 (1997).
[24] D. G. Streets and W. A. Potts, J. Chem. Soc. Faraday II **70**, I505 (1971).
[25] E. Lindholm and L. Asbrink, J. Electron. Spectrosc. **18**. 121 (1980).
[26] U. Gelius, E. Bailier, S. Svensson, T. Bergmark, and K. Siegbahn, J. Electron. Spectrosc. **2**, 405 (1974).

[27] W. von Niessen, L. S. Cedcrbaum, and W. P. Kraemar, J. Chem. Phys. **65**, 1378 (1976).
[28] K. Hirao and H. Kato, Chem. Phys. Lett. **98**, 340 (1983).
[29] L. S. Cederbaum, W. Domcke, I. Schirmer, W. von Niessen, G. H. F. Diercksen, and W. P. Kraemar, J. Chem. Phys. **69**, 1591 (1978).
[30] I. Fuss, I. E. McCarthy, A. Minchinton, and E. Weigold, Chem. Phys. **63**, 19 (1981).
[31] O. Samardzic, M. J. Brunger, A-M. Grisogonot, and E. I. Weigold, J. Phys. B **26**, 3921 (1993).
[32] X. G. Ren, C. G. Ning, J. K. Deng, S. F. Zhang, G. L. Su, F. Huang, and G. Q. Li, Rev. Sci. Instrum. **76**, 063103 (2005).
[33] X. G. Ren, C. G. Ning, J. K. Deng, S. F. Zhang, G. L. Su, B. Li, and X. J. Chen, Chin. Phys. Lett. **22**, 1382 (2005).
[34] C. G. Ning, S. F. Zhang, J. K. Deng, K. Liu, Y. R. Huang, and Z. H. Luo, Chin. Phys. B **17**, 1729 (2008).
[35] K. Liu, C. G. Ning, Z. H. Luo, L. L. Shi, and J. K. Deng, Chem. Phys. Lett. **497**, 229 (2010).
[36] H. Nakatsuji, Chem. Phys. Lett. **59**, 362 (1978).
[37] H. Nakatsuji and K. Hirao, Int. J. Quantum Chem. **20**, 1301 (1981).
[38] A. D. Becke, J. Chem. Phys. **98**, 5648 (1993).
[39] C. Lee, W. Yang, and R. G. Parr, Phys. Rev. B **37**, 785 (1988).
[40] Y. R. Miao, C. G. Ning, and J. K. Deng, Phys. Rev. A **83**, 062706 (2011).
[41] Y. R. Miao, J. K. Deng, and C. G. Ning, J. Chem. Phys. **136**, 124302 (2012).
[42] Y. R. Miao, C. G. Ning, K. Liu, and J. K. Deng, J. Chem. Phys. **134**, 204304 (2011).
[43] M. J. Frisch, G. W. Trucks, H. B. Schlegel, G. E. Scuseria, M. A. Robb, J. R. Cheeseman, J. A. Jr. Montgomery, T. Vreven, K. N. Kudin, J. C. Burant *et al.*, GAUSSIAN 03, Revision E.01, Gaussian, Inc., Wallingford, CT, 2004.
[44] C. G. Ning, B. Hajgató, Y. R. Huang, S. F. Zhang, K. Liu, Z. H. Luo, S. Knippenberg, J. K. Deng, and M. S. Deleuze, Chem. Phys. **343**, 19 (2008).
[45] I. E. McCarthy and E. Weigold, Rep. Prog. Phys. **51**, 299 (1988).
[46] M. J. Brunger, S. W. Braidwood, I. E. McCarthy, and E. Weigold, J. Phys. B **27**, L597 (1994).
[47] C. E. Brion, Y. Zheng, J. Rolke, J. J. Neville, I. E. McCarthy, and J. Wang, J. Phys. B **31**, L223 (1998).
[48] J. S. Zhu, Y. R. Miao, J. K. Deng, and C. G. Ning, J. Chem. Phys. **137**, 174305 (2012).
[49] N. Watanabe, M. Yamazaki, and M. Takahashi, J. Electron Spectrosc. Relat. Phenom. **209**, 78 (2016).
[50] N. Watanabe, M. Yamazaki, and M. Takahashi, J. Chem. Phys. **137**, 114301 (2012).
[51] B. Hajgato, F. Morini, and M. S. Deleuze, Theor. Chem. Acc. **131**, 1244 (2012).
[52] J. Yang, X. Shan, Z. Zhang, Y. Tang, M. Zhao, and X. J. Chen, J. Phys. Chem. A **118**, 11780 (2014).
[53] N. Watanabe, M. Yamazaki, and M. Takahashi, J. Chem. Phys. **141**, 244314 (2014).
[54] F. Morini, M. S. Deleuze, N. Watanabe, and M. Takahashi, J. Chem. Phys. **142**, 094308 (2015).
[55] F. Morini, N. Watanabe, M. Kojima, M. S. Deleuze, and M. Takahashi, J. Chem. Phys. **143**, 134309 (2015).
[56] Y. Tang, X. Shan, J. Yang, S. Niu, Z. Zhang, N. Watanabe, M. Yamazaki, M. Takahashi, and X. J. Chen, J. Phys. Chem. A **120**, 6855 (2016).
[57] S. B. Zhang, X. Y. Li, J. G.Wang, Y. Z. Qu, and X. Chen, Phys. Rev. A **89**, 052711 (2014).
[58] X. Li, M. Gong, L. Liu, Y. Wu, J. Wang, Y. Qu, and X. Chen, Phys. Rev. A **95**, 012703 (2017).
[59] X. Li, X. Ren, K. Hossen, E. Wang, X. J. Chen, and A. Dorn, Phys. Rev. A **97**, 022706 (2018).